Applied Physics Letters

Cross-shaped nanostructures for the study of spin to charge inter-conversion using spin-orbit coupling in non-magnetic materials

Cite as: Appl. Phys. Lett. **114**, 222401 (2019); https://doi.org/10.1063/1.5078957
Submitted: 29 October 2018 . Accepted: 14 May 2019 . Published Online: 04 June 2019

V. T. Pham, L. Vila, G. Zahnd, P. Noël, A. Marty, and J. P. Attané

AIP Publishing

Applied Physics Letters ARTICLE scitation.org/journal/apl

Cross-shaped nanostructures for the study of spin to charge inter-conversion using spin-orbit coupling in non-magnetic materials

Cite as: Appl. Phys. Lett. **114**, 222401 (2019); doi: 10.1063/1.5078957
Submitted: 29 October 2018 · Accepted: 14 May 2019 ·
Published Online: 4 June 2019

V. T. Pham,[1,a)] L. Vila,[1,b)] G. Zahnd,[1,2] P. Noël,[1] A. Marty,[1] and J. P. Attané[1,c)]

AFFILIATIONS

[1]Université Grenoble Alpes, CEA, CNRS, INP-G, IRIG-Spintec, F-38054 Grenoble, France
[2]Hprobe, 4 Rue Irène Joliot-Curie, 38320 Eybens, France

[a)]**Current address:** CIC nanoGUNE, 20018 Donostia-San Sebastián, Basque Country, Spain.
[b)]laurent.vila@cea.fr
[c)]jean-philippe.attane@cea.fr

ABSTRACT

Several spin–orbit effects allow performing spin to charge interconversion due to the spin Hall effects or the spin-momentum locking at Rashba interfaces and topological insulator surface states. Here, we focus on how these interconversions can be made electrically, using three different cross-shaped nanostructures. We apply the measurement configurations to the case of the spin Hall effect in Pt using CoFe electrodes to detect or inject spins. Both the direct and inverse spin Hall effects can be detected, with spin Hall signals up to two orders of magnitude higher than that of nonlocal measurements in metallic lateral spin valves, and with a much simpler fabrication protocol. We compare the respective signal amplitude of the three proposed geometries. Finally, we show that finite element method calculations allow extracting the spin Hall angle and the spin diffusion length of Pt from these measurements.

Spin current manipulation is at the core of spintronics. The spin–orbit interaction (SOI) in nonmagnetic materials is now being considered to create and detect spin currents. For instance, the spin Hall effect (SHE) and its inverse[1] allow performing the interconversion between charge and spin currents in bulk materials.[2] Edelstein Rashba effects, at interfaces or on the surfaces of topological insulators, can also ensure these interconversions and be highly competitive.[3]

The direct SHE (DSHE) converts a charge current into a transverse pure spin current, a flow of spin angular momentum without net charge flow. The relationship between the produced pure spin current ($\mathbf{J_s}$), the charge current ($\mathbf{J_c}$), and the spin polarization of electrons ($\mathbf{s}$) can be written as $\boldsymbol{J_S} = \frac{\hbar}{e}\Theta_{SHE}\,\boldsymbol{J_C} \times \boldsymbol{s}$,[1] where the conversion rate θ_{SHE} is the spin Hall angle of the considered material. Reciprocally, a transverse charge current is generated from a spin current by the reverse mechanism, with the same conversion rate.

A lot of techniques have been devoted to SHE detection, such as the ferromagnetic resonance (FMR)-based spin pumping/spin torque techniques,[4–6] the spin Hall magnetoresistance,[7] optical schemes,[8,9] and electrical techniques on nanodevices.[10,16,20] Nanostructures that allow detecting the SHE electrically are of prime interest in view of SO-based logic devices[11] and nonvolatile magnetic random access memories (MRAMs),[12] altogether with applications in spin–orbit torque experiments.[13,14]

Among electrical methods, nonlocal techniques based on lateral spin valves (LSVs)[15,16] are playing a significant role in SHE research works. However, their straightforward use is hampered by the complexity of nanostructure fabrication and by the smallness of the spin signals, especially for metallic systems.

Electrical devices that can produce high spin signals are thus of prime importance not only for the basic research, but also for applications. Recently, we proposed a simple F/N bilayer device, in which two ferromagnetic electrodes directly probe the spin accumulation induced in an underneath SHE nanowire, thus achieving large spin-charge interconversion signals.[17] In this paper, we propose and compare alternative cross-shaped nanostructures allowing DSHE and inverse SHE (ISHE) measurements. Taking advantage of the local spin measurement technique, these devices can be scaled down to produce high DSHE/ISHE signals in the 10 mΩ range at room temperature, up to two orders of magnitude larger than those of typical metallic nonlocal devices. Moreover, they possess a much simpler structure that could be

implemented in SHE-based computational devices.[11,12] Finally, we will show that they allow measuring the spin Hall angle, using Finite Element Method (FEM) simulations.

The samples have been fabricated by conventional e-beam lithography, e-gun deposition, and lift-off processes on the thermally oxidized SiO_2/Si substrate. The chosen materials are $Co_{60}Fe_{40}$ and Pt, as they are archetypal ferromagnetic and SHE materials. We have characterized their magnetic and spin transport properties.[17,18] The material depositions have been performed at 4×10^{-8} mTorr. The Pt strips have been deposited first. Their top surface is cleaned by Ar ion etching prior to the deposition of the top CoFe electrodes. These nanowires are connected to Ti\Au electrical pads. In all the samples, the thickness of the CoFe layer is 15 nm, whereas that of the Pt layer is 7 nm for the device in Fig. 1(a) and 8 nm for the samples in Figs. 1(c) and 1(e). The widths of the CoFe and Pt nanowires are 50 nm and 400 nm, respectively. The measurements have been performed using a lock-in technique, with an applied current of 100 or 200 μA.

Figures 1(a), 1(c), and 1(e) show the SEM images and the measurement configuration for DSHE, and the corresponding ISHE measurement principles are sketched in Figs. 1(b), 1(d), and 1(f). In all the experiments, the spin signal (in Ohm) is the ratio between the detected voltage and the applied current. The external magnetic field is applied along the easy axis of the ferromagnetic electrodes.

Figures 1(a) and 1(b) correspond to the two-probe device proposed in Ref. 17. In Fig. 1(a), a vertical (along Z) pure spin current is created by DSHE when a charge current flows along the Pt wire. The spin accumulation created by this pure spin current is probed by the two CoFe electrodes, providing that the magnetizations of the two ferromagnetic-electrodes are opposite. If these magnetizations are parallel, they probe the same electrochemical potential, so that the spin signal is null. In the reciprocal configuration of Fig. 1(b) and when the two magnetizations of the CoFe electrodes are opposite, the spin currents injected at the CoFe/Pt interfaces have identical signs. This generates the conversion by ISHE of a nonzero net transverse charge current along the Pt wire. Under open circuit conditions, this transverse charge current results in the voltage V_{SHE}.

This nanostructure can be simplified as shown in Figs. 1(c) and 1(d), with a single CoFe electrode connected to the top of a T-shaped pattern made of Pt. In Fig. 1(c), the charge current flowing in the Pt creates a spin accumulation on its top surface. The transverse ferromagnetic contact probes this spin accumulation, by measuring the associated split of electrochemical potential at the CoFe/Pt top interface. Indeed, the ferromagnetic electrode probes the electrochemical potential of minority or majority spins, depending on its magnetization orientation. The ISHE can be measured by permuting the current and voltage leads [Fig. 1(d)]. The charge current flowing at the CoFe/Pt interface allows the injection of a spin current. This spin current is converted into a transverse charge current by ISHE, which leads to a transverse voltage under open circuit conditions. The direction of the produced charge current is reversed when the polarization of the spin current changes with the reversal of the magnetization of the ferromagnetic electrode.

Finally, Figs. 1(e) and 1(f) illustrate a simple cross, made of two straight CoFe and Pt wires. It can be seen as a reference device: in the presented electrical set-up, the spin signal is expected to be zero whatever the magnetization direction of the ferromagnetic electrode. We will show later that when using a different electrical set-up, this last and simplest configuration also allows measuring ISHE and DSHE spin signals, although with a large signal offset.

The spin signals corresponding to the DSHE and ISHE configurations of these three devices are plotted in Figs. 2(a), 2(c), and 2(e) and Figs. 2(b), 2(d), and 2(f), respectively. All the figures have the same range of signal amplitude to ease their direct comparison. Drops and rises in the spin signal correspond to the magnetization reversals of the CoFe electrodes. In the DSHE configuration, magnetization switching leads to a change in the probed electrochemical potential, from majority to minority spins, or vice-versa. In the ISHE configuration, it leads to the change in polarization of the injected spin current. The spin signal amplitude is defined as the maximal variation of the signal during the loop.

Unlike nonlocal techniques, the local spin detection has no need for a spin transport channel, (i) reducing the spin relaxations (in the spin channel and at its two contacts) and (ii) avoiding electrical shunting by the high conducting spin channel, so that it allows achieving spin to charge interconversion in a more confined geometry, with an expectedly higher spin signal amplitude.[19] Indeed, these simple nanostructures show that the absolute value of the spin-to-charge signal is in the 10 mΩ range at room temperature, around two orders of magnitude larger than in the standard nonlocal measurement in the metallic lateral spin valve.[15,20,21] Beyond the device principle, the spin signals also benefit from the quality of CoFe as a spin injector in Pt, in comparison with the more commonly used NiFe.[18]

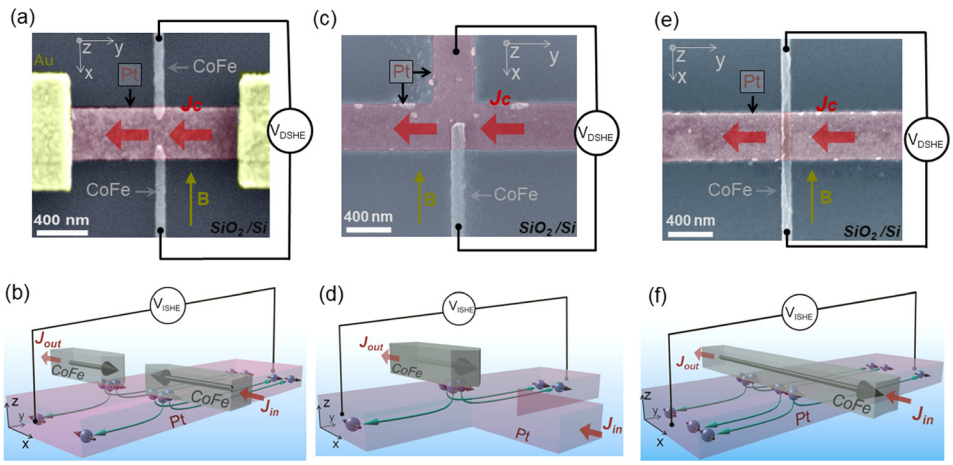

FIG. 1. (a), (c), and (e) Colored SEM images of the studied devices, with the electrical set-ups corresponding to SHE measurements. The CoFe ferromagnetic electrodes appears in gray and the Pt ones in purple. In (e), the injected spin current is, on average, zero. The external magnetic field (yellow arrow) controls the magnetization in the ferromagnetic electrode, represented by black arrows. (b), (d), and (f) Sketches of the devices showing the ISHE measurement setups.

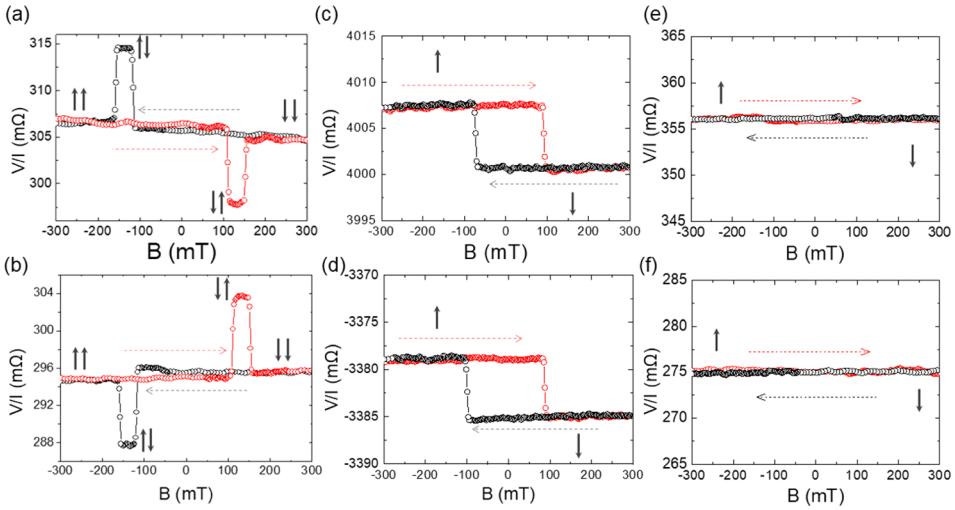

FIG. 2. (a)–(f) The spin signals obtained for DSHE and ISHE experiments corresponding to the measurement schemes shown in Figs. 1(a)–1(f), respectively. The black arrows represent the magnetization states. Red (or black) half-loops correspond to increasing (or decreasing) fields.

As is expected from the ISHE and DSHE reciprocity, the obtained spin signal amplitudes are similar. The small offset resistance can be explained by slight misalignments between different electrodes or inhomogeneities of the charge current lines. The results illustrated in Figs. 2(a) and 2(b) correspond to the device geometry in Ref. 17. The two electrodes have different switching fields, and the spin signal amplitude is about 16 mΩ. It is larger by nearly a factor of 2 than the 7 mΩ spin signal amplitude of the device shown in Figs. 2(c) and 2(d). Indeed, in the measurements of Figs. 2(a) and 2(b), the spin current is injected twice at the ferromagnetic/non-magnetic (FM/NM) interface in ISHE (or the spin accumulation is measured twice in DSHE), and the signal amplitude is thus roughly a factor of 2 larger than when there is only one electrode. If its spin signal amplitude is reduced, the geometry of Figs. 1(c) and 1(d) has nonetheless a larger tolerance to overlay alignment errors, and might thus be easier to fabricate and scale down. This geometry is close to the one proposed in the magneto-electric spin-orbit (MESO) concepts recently introduced by Intel in Ref. 11.

Figures 2(e) and 2(f) illustrate the spin signal loops corresponding to the geometry device and probe configurations of Figs. 1(e) and 1(f), respectively. As is expected, zero spin signal is obtained in both cases. In the DSHE configuration, the same electrochemical potential is probed along the ferromagnetic wire [Fig. 2(e)]. In the ISHE configuration, the injected spin current into the Pt wire is zero on average, thus producing no transverse voltage.

As is shown in Fig. 3, these cross-shaped nanostructures can also be used to study the spin signal in other probe configurations, depicted in the insets. Compared to the ones presented in Fig. 2, these measurement configurations give a larger offset, decreasing the signal/noise ratio, and they also show a smaller signal. In Figs. 3(a) and 3(b), the current flows through one CoFe/Pt interface, generating a spin accumulation like in an ISHE configuration, while the other CoFe/Pt interface probes the spin accumulation, like in a DSHE configuration. The spin signal is thus a combination of DSHE and ISHE signals.

The spin signal amplitude, around 7 mΩ, is roughly two times lower than that of Figs. 2(a) and 2(b): indeed, the current

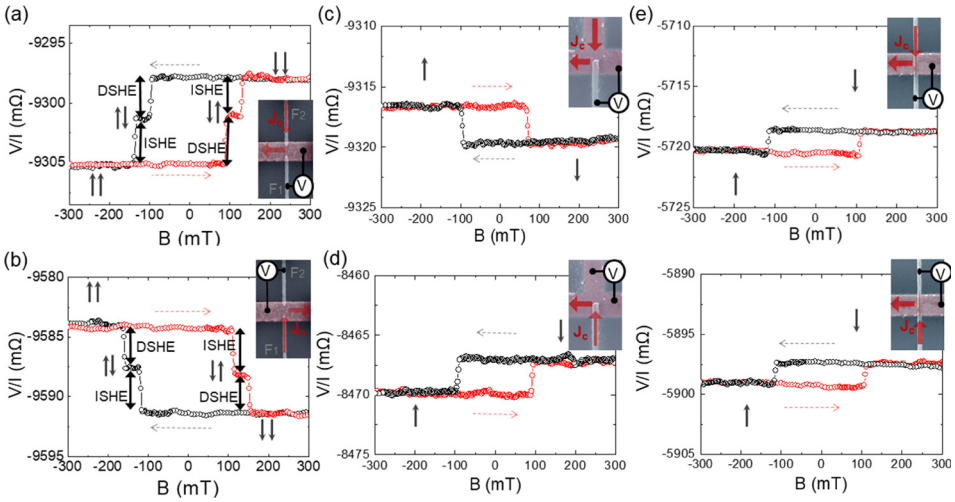

FIG. 3. Spin signals measured using alternate measurement configurations (shown in the inset). In (a) and (b), the switching field of electrode F1 is smaller than that of electrode F2.

flows through only one interface. A similar behavior can be observed in the T-shaped device. The spin signal amplitudes in Figs. 3(c) and 3(d) are roughly a factor of 2 smaller than those in Figs. 2(c) and 2(d) (3 mΩ vs 7 mΩ).

Remarkably, the probe configuration of Figs. 3(e) and 3(f) now allows observing a signal for the simplest device, with the straight CoFe wire. This configuration has already been used in experiments involving topological insulators.[22–24] The results can be explained by using the same mechanism as in Figs. 3(a) and 3(b), i.e., the signal is a combination of both DSHE and ISHE. However, there is no distinction between DSHE and ISHE contributions in the signal here because both the injection and detection zones have the same magnetization direction. Additionally, because the ferromagnetic-wire is continuous, the transverse resistance is decreased, and the spin signal amplitude is much reduced compared to the results of Figs. 3(a) and 3(b), where the CoFe wire does not fully cover the Pt strip.

In order to confirm that the measured signals originated mainly from the SHE of Pt, we carried out finite element method simulations, similarly to what has been done in Ref. 17 within the framework of a 2 spin-current drift diffusion model.[25] For a magnetization axis along X, the spin current densities can be written as

$$\vec{J}_{\uparrow/\downarrow} = \begin{pmatrix} 1 & 0 & 0 \\ 0 & 1 & \pm\Theta_{SHE} \\ 0 & \mp\Theta_{SHE} & 1 \end{pmatrix} \frac{1 \pm p_F}{2\rho} \vec{\nabla}\mu_{\uparrow/\downarrow}, \quad (1)$$

$$\vec{J}_c = \vec{J}_\uparrow + \vec{J}_\downarrow, \quad (2)$$

where $\vec{J}_{\uparrow/\downarrow}$ and $\mu_{\uparrow/\downarrow}$ are the current densities and electrochemical potentials of spin-up and spin-down electrons, respectively. Note that the anomalous Hall effect (AHE),[26] the most possible artifact that could mimic the spin Hall signals, is carefully taken into account in the simulations. In ferromagnetic materials, Eqs. (1) and (2) stand for the anomalous Hall effect, its angle being defined as $\Theta_{AHE} = p_F \Theta^F_{\mathrm{SHE}}$, where Θ^F_{SHE} is the spin Hall angle of ferromagnetic materials (for CoFe, $\Theta_{AHE} = 0.63\%$). In Pt, the polarization in Eq. (1) is zero. More details on the simulations are provided in Ref. 17.

The T-shaped device presented in Fig. 1(c) has the advantage of showing a much larger signal than that of the straight wires, with a smaller voltage offset, and with the fabrication process being less stringent in an overlay alignment than that of the two-electrode device [Fig. 1(a)] and measurement schemes presented in Fig. 3. This device and the measurement setup are chosen for the representation of the simulation in Fig. 4. The distribution of the applied charge current of Fig. 4(a) allows injecting a spin polarized current in the Z-direction at the CoFe/Pt interface. The spin accumulation landscape is shown in Figs. 4(b) and 4(c). The spin accumulation is large in the vicinity of the CoFe/Pt interface where the charge current crosses the interface. The calculations have been done using the experimentally measured resistivities ($\rho_{Pt} = 28\ \mu\Omega$ cm for 8 nm thick Pt and $\rho_{CoFe} = 20.5\ \mu\Omega$ cm for 15 nm thick CoFe[27]). The spin diffusion length is taken to be $\lambda_{Pt} = 3.0$ nm, equal to that measured in Ref. 17. Table I reports the calculated spin signal (ΔR_{SIM}) and the AHE signal ($\Delta R_{\mathrm{SIM\_AHE}}$) according to the device type and measurement setup as given in column 1. The experimentally measured signal (ΔR_{Exp}) is given in the last column.

The simulations show very good agreement with the measured spin signal amplitudes (ΔR_{Exp}), if we used the Pt effective spin Hall angle of Ref. 17 ($\Theta_{SHE} = 0.19 \pm 0.01$). A negligible contribution (less than 5% in most cases) of AHE is found, whatever the geometry of the devices. Particularly, the simulation shows that the contribution of the AHE is minimized in the nanostructures having the thickness of the CoFe electrode about two times that of the Pt layer.[28] The minus sign of $\Delta R_{\mathrm{SIM\_AHE}}$ indicates that the AHE can even have a negative contribution to the spin signals.[28] This good agreement between simulated and experimental data allows concluding that the obtained spin signals mainly originated from the SHE (more than 95% in most cases), and that all of the device configurations can be used to study the spin-charge interconversion. For practical purposes, it is worth stressing that the output signal expressed in Ohms (V/I) evolves as the inverse of the width of the Pt stripe. A maximum is also found when the thickness of the Pt stripe is two times its spin diffusion length. In contrast, in terms of output voltage at a fixed current density, the

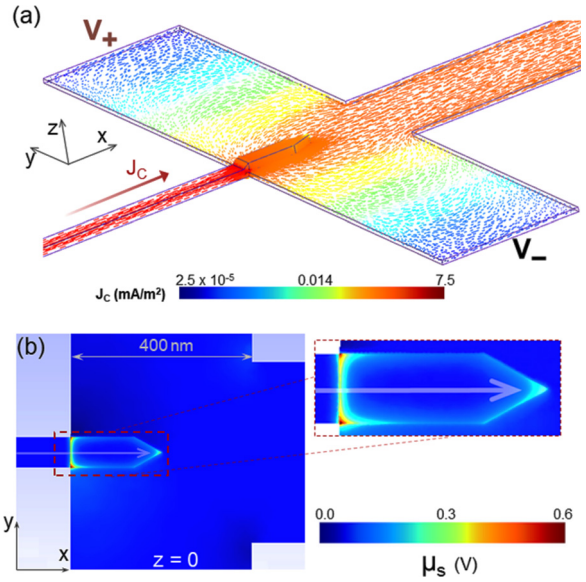

FIG. 4. (a) Charge current lines calculated by finite element method simulations for the sample of Fig. 1(d), showing the spread of the current line in the Pt strip. The charge current is applied in the X-direction, along the ferromagnetic electrode, and through the Pt wire. (b) Map of the electrochemical potential contour in the X–Y plane at the interface (z = 0). The electrode magnetization appears as a gray arrow.

TABLE I. 3D finite element method (FEM) simulation results of the spin Hall signal amplitude (ΔR_{SIM}) and the contribution of AHE ($\Delta R_{\mathrm{SIM\_AHE}}$) as well as the experimentally measured signal (ΔR_{Exp}) according to the configuration given in the first column.

Results in figures	ΔR_{SIM} (mΩ)	$\Delta R_{\mathrm{SIM\_AHE}}$ (mΩ)	ΔR_{Exp} (mΩ)
Figures 2(a) and 2(b)	±7.4	0.10	±8.0 ± 0.6
Figures 2(c) and 2(d)	6.8	−0.06	7.0 ± 0.4
Figures 2(e) and 2(f)	0.0	0.00	0.0 ± 0.6
Figures 3(a) and 3(b)	6.3	0.03	6.7 ± 0.5
Figures 3(c) and 3(d)	3.0	−0.09	3.0 ± 0.5
Figures 3(e) and 3(f)	2.42	−0.24	2.2 ± 0.6

maximum will occur for a Pt-thickness being equal to its spin diffusion length. This allows one to determine the spin diffusion length, while the only remaining unknown parameter would be the spin Hall angle.

To conclude, we studied three cross-shaped nanostructures allowing spin-charge interconversion measurements. The spin signals obtained in these local techniques are in the 10 mΩ range, in the DSHE and ISHE configurations. We also showed that we can measure DSHE and ISHE in a simple junction between two CoFe and Pt wires, and that the FEM simulations can be performed to extract the spin current/charge current conversion rate. Apart from providing simple techniques for the metrology of the SHE/ISHE, these results are also a step toward the development of computational magnetic devices, such as a nonvolatile memory with a single nano-magnet[12] or spin–orbit based logic circuits.[11] Finally, we emphasize that these device geometries, in particular, the T-shaped, can also be used to study the spin-charge interconversion at Rashba interfaces or surfaces of topological insulators.

The devices were fabricated at Plateforme Technologique Amont in Grenoble, and support from the Renatech network is acknowledged. We acknowledge the support from the LABEX laboratory LANEF (No. ANR-10-LABX-51-01) of Univ. Grenoble Alpes and funding from the ANR TOPRISE (No. ANR-16-CE24-0017).

REFERENCES

[1]E. Hirsch, Phys. Rev. Lett. **83**, 1834 (1999).
[2]A. Hoffmann, IEEE Trans. Magn. **49**, 5172–5193 (2013).
[3]A. Soumyanarayanan, N. Reyren, A. Fert, and C. Panagopoulos, Nature **539**, 509 (2016).
[4]A. Manchon, H. C. Koo, J. Nitta, S. M. Frolov, and R. A. Duine, Nat. Mater. **14**, 871 (2015).
[5]Y. Tserkovnyak, A. Brataas, and G. E. Bauer, Phys. Rev. Lett. **88**, 117601 (2002).
[6]E. Saitoh, M. Ueda, H. Miyajima, and G. Tatara, Appl. Phys. Lett. **88**, 182509 (2006).
[7]C. O. Avci, K. Garello, A. Ghosh, M. Gabureac, S. F. Alvarado, and P. Gambardella, Nat. Phys. **11**, 570 (2015).
[8]V. Sih, R. C. Myers, Y. K. Kato, W. H. Lau, A. C. Gossard, and D. D. Awschalom, Nat. Phys. **1**, 31 (2005).
[9]J. Wunderlich, B. G. Park, A. C. Irvine, L. P. Zârbo, E. Rozkotová, P. Nemec, V. Novák, J. Sinova, and T. Jungwirth, Science **330**, 1801 (2010).
[10]E. S. Garlid, Q. O. Hu, M. K. Chan, C. J. Palmstrøm, and P. A. Crowell, Phys. Rev. Lett. **105**, 156602 (2010).
[11]S. Manipatruni, D. E. Nikonov, C. C. Lin, T. A. Gosavi, H. Liu, B. Prasad, Y. L. Huang, E. Bonturim, R. Ramesh, and I. A. Young, Nature **565**, 35 (2019).
[12]S. Sayed, S. Hong, E. E. Marinero, and S. Datta, IEEE Electron Device Lett. **38**, 1665 (2017).
[13]I. M. Miron, G. Gaudin, S. Auffret, B. Rodmacq, A. Schuhl, S. Pizzini, J. Vogel, and P. Gambardella, Nat. Mater. **9**, 230–234 (2010).
[14]L. Liu, C. F. Pai, Y. Li, H. W. Tseng, D. C. Ralph, and R. A. Buhrman, Science **336**, 555 (2012).
[15]T. Kimura, Y. Otani, T. Sato, S. Takahashi, and S. Maekawa, Phys. Rev. Lett. **98**, 156601 (2007).
[16]S. O. Valenzuela and M. Tinkham, Nature **442**, 176 (2006).
[17]V. T. Pham, L. Vila, G. Zahnd, A. Marty, W. Savero-Torres, M. Jamet, and J. P. Attané, Nano Lett. **16**, 6755–6760 (2016).
[18]G. Zahnd, L. Vila, V. T. Pham, A. Marty, P. Laczkowski, W. S. Torres, C. Beigné, C. Vergnaud, M. Jamet, and J. P. Attané, Nanotechnology **27**, 035201 (2016).
[19]H. Jaffrès, J.-M. George, and A. Fert, Phys. Rev. B **82**, 140408(R) (2010).
[20]L. Vila, T. Kimura, and Y. Otani, Phys. Rev. Lett. **99**, 226604 (2007).
[21]M. Morota, Y. Niimi, K. Ohnishi, D. H. Wei, T. Tanaka, H. Kontani, T. Kimura, and Y. Otani, Phys. Rev. B **83**, 174405 (2011).
[22]C. H. Li, O. M. J. van't Erve, J. T. Robinson, Y. Liu, L. Li, and B. T. Jonker, Nat. Nanotechnol. **9**, 218 (2014).
[23]J. Tang, L. Chang, X. Kou, K. I. Murata, E. S. Choi, M. Lang, Y. Fan, Y. Jiang, M. Montazeri, W. Jiang, Y. Wang, L. He, and K. L. Wang, Nano Lett. **14**, 5423 (2014).
[24]Y. Ando, T. Hamasaki, T. I. Kurokawa, K. Ichiba, F. Yang, M. Novak, S. Sasaki, K. Segawa, Y. Ando, and M. Shiraishi, Nano Lett. **14**, 6226 (2014).
[25]T. S. Kim, B. C. Lee, and H. W. Lee, Phys. Rev. B **78**, 214427 (2008).
[26]N. Nagaosa, J. Sinova, S. Onoda, A. H. MacDonald, and N. P. Ong, Rev. Mod. Phys. **82**, 1539 (2010).
[27]G. Zahnd, L. Vila, V. T. Pham, M. Cosset-Cheneau, W. Lim, A. Brenac, P. Laczkowski, A. Marty, and J. P. Attané, Phys. Rev. B **98**, 174414 (2018).
[28]V. T. Pham, "Ferromagnetic/nonmagnetic nanostructures for the electrical measurement of the spin Hall effect and the detection of domain walls," Ph.D. thesis, Univ. Grenoble Alpes, 2016.